PAPER

Check for updates

Physical aging and evolution of mechanical properties of additively manufactured polyethylene terephthalate glycol†

Sierra F. Yost,[a] Jordan C. Smith,[b] Christian W. Pester [ID][c] and Bryan D. Vogt [ID] *[a]

Near net shape manufacture *via* material extrusion (MEX) of thermoplastics tends to rely on glassy amorphous polymers to avoid stresses generated from crystallization. Polyethylene terephthalate glycol (PETG) has emerged as a high performance, low-cost feedstock for MEX. Crystallization in PETG is suppressed by the inclusion of cyclohexane dimethanol (CHDM) as a comonomer, but CHDM increases the segmental flexibility that can accelerate physical aging. Repeated thermal cycling during MEX printing can accelerate physical aging. Here, we investigate the aging of three commercial PETG filaments with different CHDM content. Thermal analysis demonstrated increased aging as the CHDM content in the PETG increased. Aging of additively manufactured PETG demonstrated that the process path during printing leads to a distribution of aging behavior. The thermal history is spatially dependent, leading to differences in how the PETG ages between layers and location within a printed layer. Additionally, this aging in the MEX printed PETG induced changes to the ultimate tensile stress and elongation at break that are dependent on the filament source. Accelerated aging based on time–temperature superposition demonstrated embrittlement of the printed PETG after the equivalent of 1 year of aging at 25 °C in all cases. However, an unusual increase in both strength and ductility after aging for the equivalent of 30 days of aging at 25 °C was observed with some PETG. Although print conditions are commonly optimized for mechanical performance, long-term aging behavior needs to be understood to ensure reliability of additively manufactured durable goods through their expected lifetime.

Introduction

The properties of material extrusion (MEX) additive manufactured (AM) thermoplastics depend strongly on the processing parameters with optimization of printing conditions being a common strategy to improve performance.[1–4] Generally this optimization has focused on maximizing a mechanical property, such as the elastic modulus[1] and has been reported for many plastics produced by MEX, including common filaments like poly(lactic acid) (PLA)[3] and acrylonitrile-butadiene-styrene (ABS).[4,5] However, these plastics have disadvantages in terms of poor mechanical performance (PLA) or challenges in printing (ABS). Polyethylene terephthalate glycol (PETG) has emerged as promising plastic for MEX with ease of printing (like PLA) and good mechanical performance (like ABS).[6,7] PETG is a modified copolymer of polyethylene terephthalate (PET) where up to 50% of the ethylene glycol in the PET is replaced with 1,4-cyclohexanedimethanol (CHDM).[8,9] The inclusion of CHDM disrupts the crystallization in PET and leads to a reduction in viscosity,[10] crystallinity, melting temperature, and glass transition temperature relative to PET. The CHDM content impacts properties such as alkali resistance, tensile strength, melting temperature, elongation at break, and crystallinity.[11] For 3D printing, the CHDM content in the copolymer is typically sufficient to fully suppress crystallization, but the elongation at break and tensile strength of PETG are reduced.[12]

The optimization of printed properties tends to be considered directly after printing. However, plastics are commonly exposed to environments that can alter their thermomechanical performance.[13,14] Prediction of the influence of weathering on the service life of plastics is critical to acceptance of new materials and processes in durable applications like sealants[15] and coatings.[16] Although most applications proposed for AM plastics are not outdoors, reliability in manufacturing of durable plastic goods requires consideration of polymer aging during its service life.[17] There are a plethora of external factors that can impact plastic properties over their service life.[18] For

[a]Department of Chemical Engineering, The Pennsylvania State University, University Park, PA 16802, USA. E-mail: bdv5051@psu.edu

[b]Department of Mechanical Engineering, The Pennsylvania State University, University Park, PA 16802, USA

[c]Department of Materials Science & Engineering, University of Delaware, Newark, DE, 19716, USA

example, cyclic stresses on AM PETG leads to softening of the plastic to a greater extent than with AM ABS.[19] Aging can entail three different mechanisms: chemical, biological, and physical.[20–22] Chemical aging involves a permanent change to the molecular polymer structure, such as oxidation, chain scission, or cross-linking, as a result of the environmental exposure.[23–25] For PETG, chemical aging depends on the copolymer composition as this is chemistry dependent.[26–28] Extended exposure to UV-C required for sterilization reduces mechanical performance of 3D printed PETG by nearly 30% while increasing creep compliance to reduce stability of the printed shape.[26–28] Other aging routes may impact the performance of 3D printed PETG over the lifetime of the printed part, but this area is under explored.

Physical aging is driven by the deviation from equilibrium of glasses and the small but finite mobility of polymer segments at temperatures below the glass transition temperature (T_g). This mobility promotes densification of non-equilibrium, glassy polymers towards their equilibrium density. This small but finite densification[20,22] can lead to substantial changes in mechanical performance. Unlike chemical and biological aging that can be avoided by environmental considerations, physical aging relies on finite thermal energy that slowly drives the polymer towards its equilibrium density. For glassy polymer products, some physical aging during their use is inevitable; the impact of this aging without chemical changes can lead to decreased mechanical performance long-term.[29] As comparative studies of PET, which is an analog to PETG, demonstrated that weathering over 2 years can almost exclusively be attributed to physical aging,[30] understanding these physical aging effects in AM PETG is the focus of this work.

Physical aging of polymers is impacted by a variety of factors, including process history that controls the free volume.[20,31,32] Physical aging can be considered in terms of reduction in the free volume of the polymer, where the rate of physical aging depends on the free volume present. Likewise, residual stress in a plastic can alter the aging rate,[32] but applied stress can provide mechanical rejuvenation[33] of the glass to reverse aging.[34–36] It should be noted that mechanical rejuvenation is distinct from thermal rejuvenation,[34] where heating the polymer above the glass transition recovers the initial properties of the plastic by equilibration in the melt.[21] The rate at which volume and enthalpy recover from non-equilibrium on aging tends to be different from the recovery in mechanical properties.[36]

Additives within the plastic impact the aging rate,[37] which increases complexity as additives are commonly included to reduce stresses generated and improve the inter-road adhesion in the optimization of filaments and pellets for MEX.[38] These additives depend on the manufacturer and could impact the long-term performance as a result of aging. Similarly, printing *via* MEX leads to non-equilibrium chain conformations[39] and residual stresses[40] as a result of the rapid quenching of the melt to maintain shape accuracy. These non-equilibrium conformations and stresses can lead to substantial aging of polymer glasses.[20] In general, physical aging of polymers tends

to increase ultimate tensile strength and elastic modulus, while simultaneously reducing the elongation at break.[41,42]

The relatively low T_g and flexibility of the segments in PETG make it prone to physical aging.[28,43] During MEX processing, the polymer melt is quenched through T_g to solidify the part, but this produces non-equilibrium conformations with higher volume, enthalpy, and entropy than extrapolated values from the equilibrium melt. Aging reduces free volume through densification, but this slows the rate of physical aging as the driving force (departure from equilibrium) is reduced.[22] The rate for physical aging depends on temperature with slow rates far below T_g due to limitations in the segmental mobility, while aging slows as T_g is approached as the thermodynamic driving force for aging is reduced.[20] This temperature dependence of the aging rate enables methodologies for accelerated aging, where long-term evolution of properties of the plastic at service temperatures can be predicted at shorter accessible times through time–temperature superposition (TTS).[44–46] Aging well below T_g ($T < T_g -20$ °C) tends to be slow and require long-term measurements to elucidate changes, while temperatures too close to T_g leads to non-Arrhenius behavior and breakdown of TTS.[28,43] However, intermediate temperatures enable the evolution in properties from physical aging at service temperatures over years to be predicted from TTS with measurements on the order of hours.[20] TTS has been successfully applied to PETG,[44–46] but not for 3D printed objects.

Here we report on the impact of physical aging on the properties of 3D printed PETG using a series of commercial filaments with varying CHDM content. The composition of the PETG copolymer correlates with the rate of physical aging determined from the thermometrically determined enthalpy loss. The mechanical properties of these PETG materials after 3D printing were examined as a function of aging time based on TTS determined from the thermometric measurements. Aging led to embrittlement and generally an increase in the tensile strength, but the aging induced changes were dependent on the composition of the PETG. As processing history impacts the aging behavior of other glassy polymers,[47] we compared the aging of PETG using two different printers: one designed for glassy polymers, like PLA and ABS with a long heating zone, and one designed for semicrystalline engineering plastics, like nylon and poly(ether ether ketone) (PEEK), with a small heating zone. The results demonstrate additional considerations for commercialization of additively manufactured glassy plastic parts beyond printability and initial mechanical optimization, where formulation and process changes to improve these characteristics could have unintended consequences for the long-term performance of these parts through physical aging.

Experimental section

Materials

Three commercial PETG filaments were purchased from Amazon: clear Overture (batch: A2309240165), red Hatchbox

(no batch number provided), and blue Polymaker (batch: 200915927). Manual calipers were used to measure the diameter of the filaments over 6′ of filament: 1.750 mm ± 0.011 mm for Overture, 1.738 mm ± 0.008 mm for Hatchbox, and 1.749 mm ± 0.017 mm for Polymaker. These are well within the manufacturer reported tolerances (1.75 mm ± 0.05 mm). For comparison, poly (ether ether ketone) (PEEK) filament (lot: 1130720229) with a 1.75 mm diameter was purchased from Roboze. The PEEK filament diameter was 1.735 mm ± 0.015 mm.

Material characterization

^{1}H nuclear magnetic resonance (NMR). The composition of the PETG copolymers was determined by solution ^{1}H NMR (Bruker AVIII-HD-500 MHz NMR). 3.0 mg of PETG was dissolved in 3.0 mL deuterated chloroform (Sigma Aldrich, 99.8% purity) NMR measurements used 1.0 mL from the top of the solution to avoid pigment from the filaments that sediments in chloroform. Fig. S1† illustrates the ^{1}H NMR spectra for the three PETG materials. The molar composition of copolymers is listed in Table 1. End group analysis of the NMR spectra was used to estimate the molecular mass (M_n) of the PETG in the filaments (Table 1).

Differential scanning calorimetry (DSC). Thermal characterization of the PETG was performed using a TA Instruments DSC 250 with a nitrogen (<2 ppm moisture, Linde) purge (50 mL min^{-1}). Prior to thermal analysis, the PETG was dried in a vacuum oven overnight at 75 °C. The PETG (1.0–1.5 mg) was sealed in Tzero aluminum pans. DSC measurements analyses were performed only on the second heating cycle and later to avoid impact of the thermal history of the filament. DSC thermograms were collected between 30 °C and 120 °C with a heating rate of 10 °C min^{-1} and cooling rate of 5 °C min^{-1}. T_g of the PETG was determined using the midpoint method in Trios software. Table 1 illustrates the T_g for the different PETG.

PETG aging was determined thermometrically using the DSC 250 under N$_2$ flow of 50 mL min^{-1}. Prior to measurements, the PETG was dried overnight in a vacuum oven at 75 °C and approximately 1 mg of dried PETG was sealed in the Tzero pans. The thermal history was erased by heating at 10 °C min^{-1} to 120 °C and holding at 120 °C for 3 min. The temperature was quenched to aging temperature (T_a) of 40 to 65 °C at 5 °C min^{-1} and held at the aging temperature for up to 48 h. The enthalpy recovery from physical aging was determined from integration of the heat flow greater than the baseline on heating from the aging temperature to 120 °C at 10 °C min^{-1}. This heating rate for the determining the enthalpy loss associ-

ated with aging was selected to provide good resolution without artifacts from thermal gradients.[48] This enthalpy recovery was measured as a function of aging time at the different temperature and normalized to a master curve through TTS assuming an Arrhenius relationship for the activation energy (E_a) associated with aging. The shift factor, a_T, from TTS is related to E_a, temperature for aging tested (T), and T_{ref} as:

$$a_T = \exp\left[\frac{E_a}{R}\left(\frac{1}{T_{ref}} - \frac{1}{T}\right)\right] \quad (1)$$

where R is the gas constant. The shift factor was determined from plots of the enthalpy loss *versus* time with the horizontal shift factors determined from the *x*-intercept following standard TTS protocols.

The local aging of PETG in a printed tensile bar (ASTM D638 Type IV) was determined from collection of 2–5 mg from four different locations on the specimen: the middle of the grip section from (1) the layer that contacted the print bed and (2) final printed layer as well as specimens from both top and bottom layers in the middle of the gauge section of the printed specimen. Due to the print path, each location experiences distinct thermal histories. These specimens were aged for different times and the enthalpy recovery associated with aging was quantified by on heating from 25 °C to 120 °C at 10 °C min^{-1}. The reference for the unaged sample was determined by holding the specimen at 120 °C for 3 min to erase the thermal history, cooling at 5 °C min^{-1} to 30 °C, and subsequent heating to 120 °C at 10 °C min^{-1}. The reported enthalpy loss was calculated as the difference in the integrated endotherms between the aged and erased thermal history specimens

Small angle oscillatory shear (SAOS) rheology. Small angle oscillatory shear (SAOS) measurements were performed on a TA Instruments Discovery HR 20 rheometer in parallel plate geometry with 25 mm diameter stainless steel plates and 1000 μm gap. PETG from the filaments (approximately 0.5 g, dried overnight at 75 °C) were melted at 260 °C between the plates with a gap offset of 5000 μm. Following melting, the gap was set to 1000 μm and any excess material was removed. SAOS measurements were conducted using a frequency sweep from 0.1 to 100 rad s^{-1} with 1.0% strain amplitude at temperature from 260 °C to 190 °C. TTS was applied to collapse the SAOS data to a reference temperature of 240 °C using the TRIOS software. This reference temperature is a recommended printing temperature for all filaments examined. The SAOS data were analyzed in terms of the storage and loss moduli (G', G'') and

Table 1 Composition of the PETG samples and their glass transition temperature

Source	Terephthalate (mol %)	Ethylene glycol (mol%)	CHDM (mol %)	Molar mass (kDa)	T_g (°C)
Hatchbox (H)	50	31.5	18.5	6.5	82.5
Overture (O)	50	29.0	21.0	7.1	76.2
Polymaker (P)	50	25.9	24.1	4.3	71.8

loss factor (tan δ) to compare the rheological characteristics of the different filament materials.

3D printing. Two different printers were used to print ASTM D638 type IV and type V tensile bars from the PETG filaments for assessment of the aging. Creality Ender 3 3D printer (Creality, Shenzen, China) is equipped with a long hot end (27.8 mm hot zone) that includes a 0.4 mm brass nozzle and used Cura Slicer for the g-code. The print bed temperature was 75 °C and a thin layer of glue (pen + GEAR, poly(vinyl acetate) glue stick) was applied to the bed for improved adhesion of the first printed layer of the PETG. Print speed for the Ender was 3000 mm min^{-1}.

Roboze One + Xtreme (Roboze, Apulia, Italy) has a shorter heated zone (12 mm) with a brass 0.4 mm nozzle. The Roboze printer includes a heated drying chamber to minimize moisture in the filaments. The PETG filaments were rewound on metal spools that specifically fit the drier on the Roboze printer. Filaments were dried at 75 °C overnight before use and the filament remained in the drier at 75 °C during printing to minimize exposure to atmospheric humidity. The g-code was generated from simplify 3D. A print speed of 1200 mm min^{-1} was used along with a polyetherimide bed heated to 80 °C.

For both printers, a 0.2 mm layer height, a 100% infill density, +45/−45° raster angles with a flat (x–y plane) build orientation, and 240 °C extrusion temperature was used. The nomenclature used for the printed samples is F(P)T where F refers to the filament source (H for Hatchbox, O for Overture, and P for Polymaker), P is the printer used (E for Ender and R for Roboze) and T is the type of tensile bar printed (IV or V). Due to difficulties printing PETG with the Roboze printer, only the Overture PETG filaments were printed. ASTM type IV and type V tensile bars were printed with +45/−45°, a flat (on the xy-plane) build orientation, and 100% infill.

Digital reconstruction for dimensional accuracy. The structure of the printed samples was reconstructed from blue light scanning camera (Polyga, HDI-C109) with a rotary table. Images were captured every 20° over 180° in polyga FlexScan3D software. The specimens were held on the rotatory stage during the scanning using nonhardening model clay (Sargent Art). The series of images from each scan were analysed through mesh generation to produce partial 3D images. Multiple scans were taken (2× for type V and 4× for type IV) for each specimen to fully render entire part. The meshes created from the scans were compared to CAD files of the type V or type IV tensile bars using GOM inspect 2019 software to generate false color representation of the dimensional accuracy.

Scanning electron microscopy. Scanning electron microscopy (SEM, Thermos Scientific Apreo S) operating at a beam current of 0.4 nA and a 10 kV voltage, and a working distance of 10 mm was used to characterize the cross section morphology of printed type V tensile. Specimens were prepared by cold (liquid nitrogen) fracture in the grip section and sputter coated (Leica EM ACE600) with 6 nm of iridium to minimize sample charging. Thermo Scientific Microscope Control software (v. 13.9.1) was used to analyze the SEM images.

Accelerated aging for mechanical testing. Tensile bars were aged at 60 °C for aging efficiency; this temperature maximized aging rates in traditionally manufactured PETG.[49] The aging times at 60 °C were selected to be equivalent to aging at 25 °C for 1 week, 1 month, and 1 year based on DSC measurements from aging of the PETG from the filaments. Table 3 outlines actual time used for accelerated aging at 60 °C for each material in terms of equivalent aging time at 25 °C. Aging of printed specimens was performed under vacuum at 60 °C.

Additionally, specimens at each print condition were aged for 48 h at 60 °C for comparison on an absolute scale, which is equivalent to 625.9 days, 750.7 days, and 261.9 days at 25 °C for PETG from Polymaker, Overture, and Hatchbox filaments, respectively. Five samples were examined at each aging time for the different print sizes and filaments to provide statistics in the mechanical measurements.

As exposure to humidity is typically unavoidable, the role of moisture on aging of printed Overture PETG type V tensile specimens was assessed using a Lunaire humidity chamber (Lunaire Ltd, Williamsport, PA) at 60 °C and 80% relative humidity The chamber regulated by an embedded Watlow sensor. Specimens were aged for the equivalent of 1 month and 1 year at 25 °C under dry conditions with times noted in Table 3. Direct comparison to samples aged under vacuum provided insights into the sensitivity of aging to humidity.

The tensile properties of the 3D printed PETG after various aging protocols were determined using an MTS criterion model 43 load frame equipped with a 50 kN load cell with the force during the tensile measurement recorded using TW Elite software. The design dimensions of the gauge of the tensile bar were 3.18 mm × 2.00 mm and 6.00 mm × 4.00 mm for the width and thickness of the type V and type IV tensile bars, respectively.[50] The width and thickness of the tensile samples were measured using calipers and are listed in Table 2. An MTS advantage video extensometer operating at 10 Hz was used to quantify the extension of the tensile gauge region. The crosshead speed was 0.097 cm min^{-1}, conforming to the strain rate range for ASTM D638 standard.[50]

Table 2 ASTM D638 tensile bar gauge width and height of printed samples as determined from calliper measurements

| ASTM D638 size | Hatchbox Ender (HE) | | Polymaker Ender (PE) | | Overture Ender (OE) | | Overture Roboze (OR) | |
	Width (mm)	Height (mm)	Width (mm)	Height (mm)	Width (mm)	Height (mm)	Width (mm)	Height (mm)
Type V	3.58 ± 0.10	1.88 ± 0.08	3.48 ± 0.12	1.88 ± 0.04	3.58 ± 0.16	1.86 ± 0.06	3.13 ± 0.11	2.02 ± 0.03
Type IV	6.62 ± 0.11	3.76 ± 0.06	6.54 ± 0.07	3.79 ± 0.16	6.58 ± 0.17	3.80 ± 0.05	6.00 ± 0.05	4.00 ± 0.03

Table 3 Accelerated aging times at 60 °C for each PETG filament that corresponds to desired aging times at 25 °C

Targeted aging time (t_a) @ 25 °C	Equivalent aging time @ 60 °C in h		
	Polymaker	Hatchbox	Overture
1 week	0.5	1.3	0.4
1 month	2.3	5.5	1.9
1 year	28.0	66.9	23.3

Results and discussion

Rheology defines the printability of plastic filaments,[51] but stresses from crystallization can delaminate and/or warp the print to prohibit production of the desired part.[51–53] Amorphous plastics overcome the stresses of crystallization but brittleness is a common issue. The segmental flexibility in PET provides toughness, but it is semicrystalline and can be challenging to print;[52] inclusion of >16 mol% CHDM as a comonomer is known to inhibit crystallization in PETG.[42] ^{1}H NMR demonstrates that three commercial PETG filaments contain >16 mol% CHDM and DSC thermograms confirm the lack of crystallization in these PETG filaments (Fig. S1 and S2†). CHDM increases flexibility of the polymer chain and T_g decreases as CHDM content increases as determined from DSC (Table 1). The molar masses (M_n) of the PETG were estimated from ^{1}H NMR end group analysis to be greater than the entanglement molecular weight (M_e = 3.5 kDa)[54] for all the filaments examined (see Table 1). Entanglements are required to provide mechanical strength to the printed part, but the rate of aging can be dependent on M_n.[55,56] The differences in molecular mass and CHDM composition in the PETG copolymers impact the flow characteristics of the melts during printing.

Fig. 1 illustrates the rheology of the different PETG at the recommended extrusion temperature, 240 °C. At high frequency, the storage and loss moduli are similar for all three PETG samples examined. However, the storage modulus of the Hatchbox is approximately an order of magnitude lower than the other two PETG at low frequencies despite its higher molar mass than the Polymaker filament (see Fig. 1a). As shown in Fig. 1b, the loss modulus is relatively consistent for the three filaments examined, but Hatchbox consistently exhibits the lowest loss modulus. The loss factor as shown in Fig. 1c provides some insights into rheological behavior of these PETG. All three PETG samples show a peak in tan δ as a function of frequency. As the rheological measurements are performed well above T_g but below the typical melting temperature for PET (250–260 °C), this peak could be indicative of crystalline tendencies in the PETG,[57] despite the thermal analysis indicating that the PETG is non-crystalline. Chain orientation induced by shear flow can lower barriers to crystallization.[58] The frequency dependence of the peak on the PETG source is consistent with this being related to crystalline tendencies as the peak moves to higher frequency as the concentration of
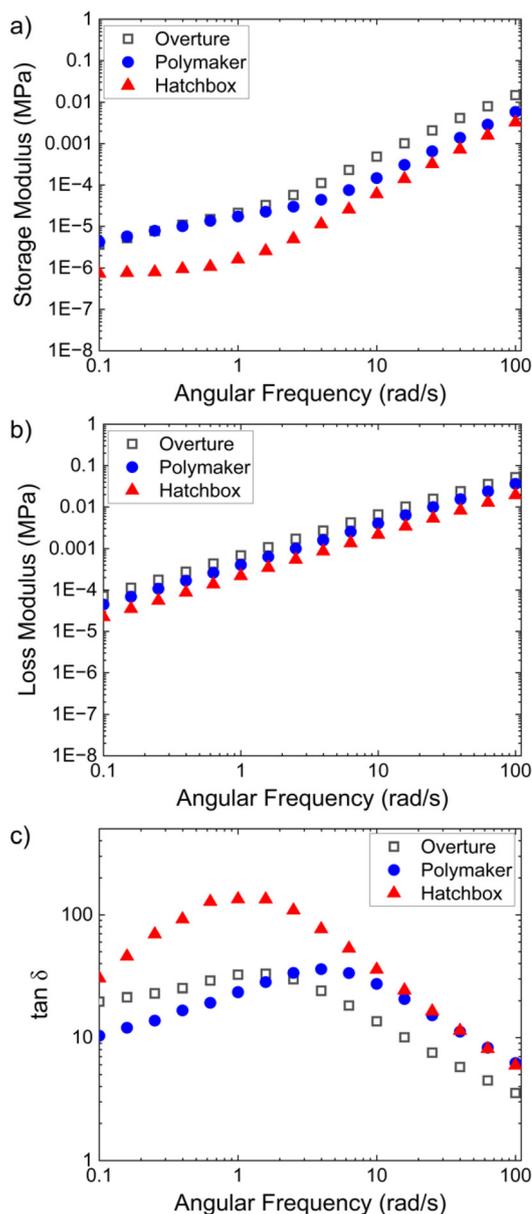
Fig. 1 (a) Storage modulus, (b) loss modulus, and (c) tan δ at 240 °C for the different PETG filaments as determined from SAOS.

CHDM in the PETG increases. CHDM reduces the potential for crystal-like association of chains due to its steric hindrance, so higher frequencies are needed as CHDM content is increased. The sharp increase in storage modulus at high frequencies, in particular for the Hatchbox PETG shown in Fig. 1a, is another indicator of reinforcement through some crystal-like associations strengthening the melt. The similarities in the rheological and thermal behaviors of the PETG filaments are not surprising as the same print conditions can be used to fabricate additively manufactured parts but the subtle differences in their rheology point to dynamic differences that may impact aging.

Physical aging of PETG

Fig. 2 illustrates the temperature dependence of physical aging of the Overture PETG as determined from the enthalpy on heating through T_g after aging between 0 and 48 h. At 40 °C, the thermograms from DSC only change marginally even after the PETG is aged 48 h as shown in Fig. 3a. This is consistent with literature for other glassy polymers where T_g −20 °C is commonly the lower limit for meaningful observed changes in the enthalpy in a reasonable experimental timeframe.[28,43] Increasing the temperature to 50 °C (Fig. 3b) changes in the thermograms on aging, where relaxation of the glass leads to densification and reduces the enthalpy. This enthalpy is recovered on heating through T_g where integration of the heat flow around T_g provides insights into the extent of physical aging. The aging rate increases further with temperature up to 60 °C (Fig. 3c). Further increases in temperature does not increase the rate of the enthalpy recovery as much because the driving force for aging (undercooling and deviation from equilibrium) is reduced (Fig. 2d).

Integration of the thermograms quantifies the enthalpy loss during aging. A denser, more energetically favorable conformation due to densification during aging leads to a detectable increase in the endotherm associated with the glass transition. Fig. 3a illustrates the integrated enthalpy as a function of aging time at temperatures from 40 °C to 65 °C for the Overture PETG. As the temperature increases, the enthalpy recovery increases more at the same aging time, which demonstrates the acceleration of aging of the PETG with temperature. These data exhibit similarities in features but shifted in time based on the aging temperature. Similar qualitative aging is observed for the other two PETG filaments as shown in Fig. S3–S6.†

TTS is used to collapse these data to a single master curve. Fig. 3b illustrates the horizontal shift factors for the collapse of the enthalpy recovery for the Overture PETG. These data demonstrate the expected Arrhenius behavior for the temperature-dependence of physical aging.[44,59] The temperature dependence of the shift factors is an effective activation energy for the glass transition, which is analogous to the activation energy for aging.[60] Similar collapse of the enthalpy recovery data through TTS is observed for the other two PETG filaments with the temperature dependence of the shift factors for the Polymaker and Hatchbox PETG shown in Fig. S4 and S6.† The activation energy (E_a) determined from the TTS Arrhenius plot was 113 kJ mol⁻¹, 125 kJ mol⁻¹, and 154 kJ mol⁻¹ for
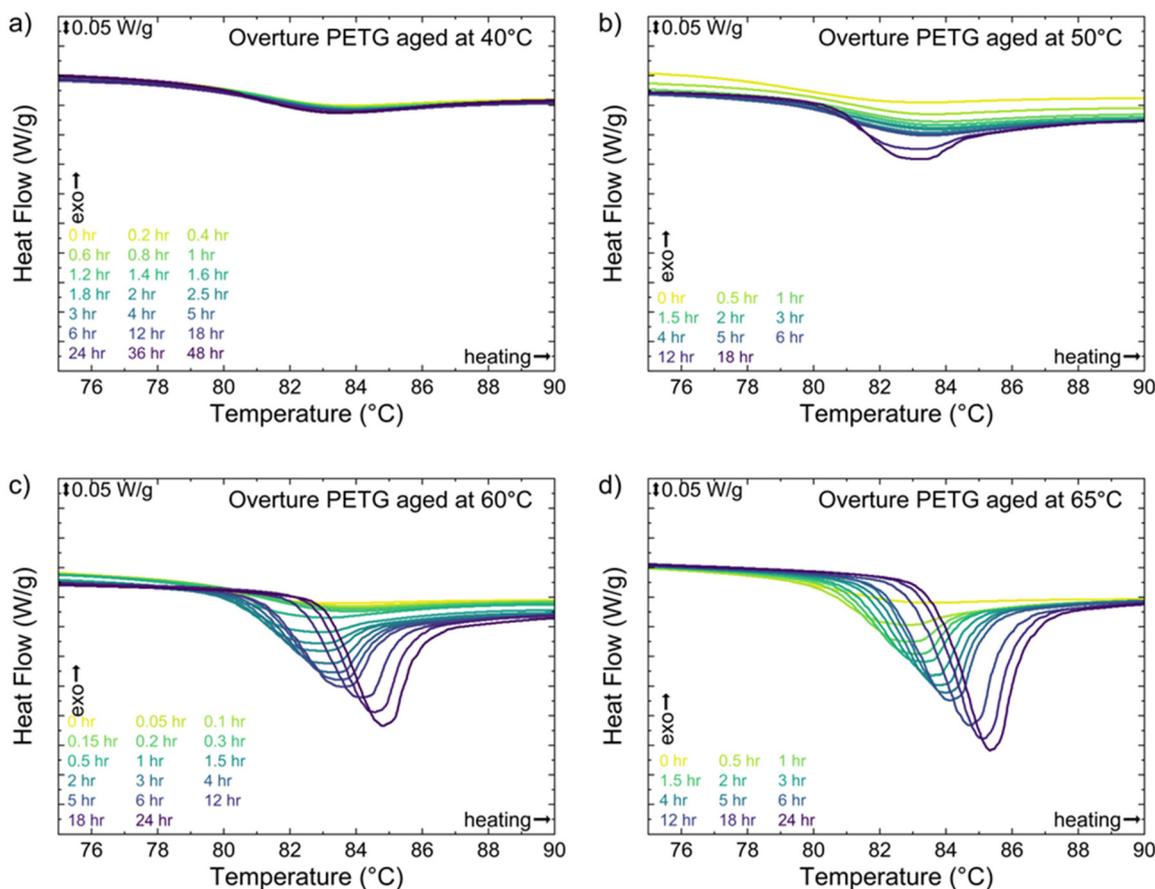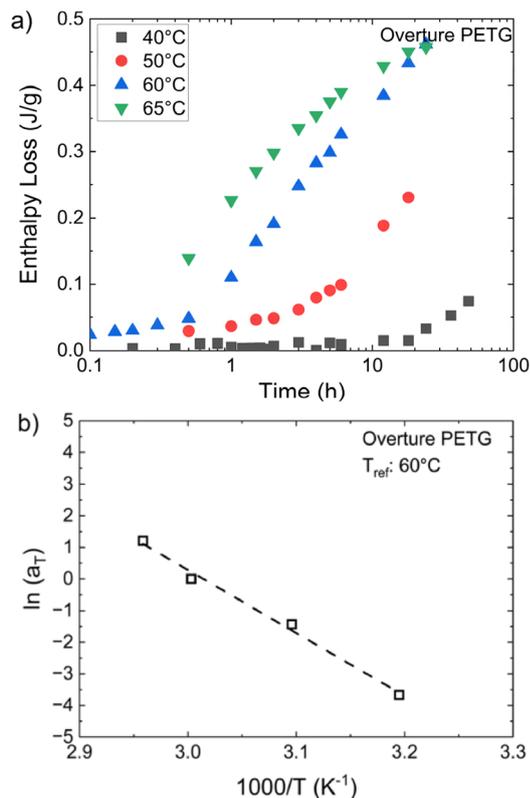

Fig. 2 DSC thermograms for Overture PETG when aged at (a) 40 °C, (b) 50 °C, (c) 60 °C, and (d) 65 °C. A constant heating rate of 10 °C min⁻¹ was used in all cases.
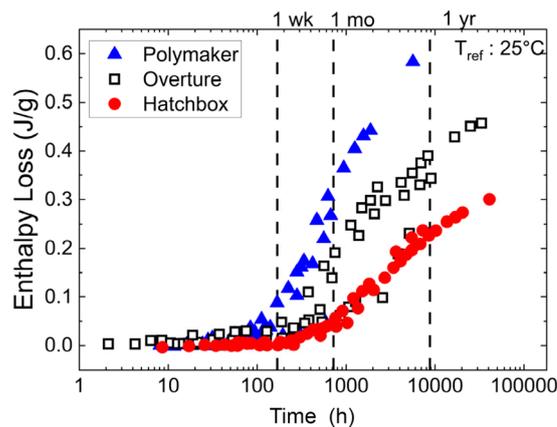
Fig. 3 (a) Enthalpy loss for Overture PETG as a function of time at different aging temperatures and (b) the Arrhenius fit of the shift factors at a reference temperature of 60 °C. The dashed line is a fit to the temperature dependence of the shift factors.

Fig. 4 Master curve at 25 °C for the aging of the PETG. TTS was used to collapse aging data at elevated temperatures to the equivalent aging at 25 °C.

Hatchbox, Polymaker, and Overture, respectively. This activation energy does not scale with molecular weight, T_g or the CHDM content. This suggests that the undeclared additives in the PETG filaments likely impact the temperature dependence of aging. At temperatures closer to T_g, the Overture PETG aging appears to equilibrate, leading to an intersection of the enthalpy loss curves in the samples aged at 60 °C and 65 °C. Accelerated aging was performed at 60 °C due to ease in assessing a broad range of enthalpy recoveries (aging states).

The measured thermograms were collapsed through TTS for each PETG sample. Fig. 4 illustrates the master curve for aging using a reference temperature of 25 °C. The noise in the enthalpy recovery is associated with the quality of the Arrhenius fit for the shift factors; as T_g is approached, alternative temperature dependencies can sometimes better describe the data such as the William–Landel–Ferry (WLF) equation.[61] With the limited temperature range examined, the goodness of the fit of the shift factors was not significantly improved by in the inclusion of additional parameters in the WLF equation, so the Arrhenius fit was used to predict long term aging of the PETG. Polymaker contains the highest CHDM content (Table 1) and ages the fastest. As the CHDM in the PETG decreases, so does the effective aging rate determined from TTS as shown in Fig. 4. This composition dependence on aging might be expected due to the increased segmental mobi-

lity imparted by the CHDM in comparison to ethylene glycol segments in the PETG.

Influence of printer selection on mechanical properties and aging

Although optimization of process conditions is commonly examined for 3D printing,[1] variations between printers that impact the quality and performance of additively manufactured parts are rarely described in the literature. Printer selection impacts precision of the gantry and thermal history based on details of the environment. The Overture PETG filament was selected for direct comparison of printing with Creality Ender 3 and Roboze One + Xtreme printers. These two printers differ in their customer base with the Creality Ender 3 being a starter printer for the hobbyist and Roboze One + Xtreme being designed to print high performance engineering plastics, such as filled nylon and PEEK, in commercial rapid prototyping operations.

Fig. 5 illustrates 3D scans of the printed PETG with the two printers. The data are presented in false color to demonstrate the deviations from the CAD design with green illustrating the regions of highest fidelity. The thermal history and imposed stresses on vitrification of the printed plastic are impacted by the size of the part.[62] The thickness of the larger type IV tensile bars (Fig. 5a) printed with the Ender is greater than the design with the largest deviations at the transitions between the gauge and grip regions of the dog bone. The smaller type V bar (Fig. 5b) shows more limited deviation from the model with the Ender printer. The direct drive in the Roboze printer provides improved accuracy to the parts for both the type IV (Fig. 5c) and type V (Fig. 5d) tensile bars when compared with those printed with the Ender. However, there are clear print path features visible near the perimeter in Fig. 5d, which suggests imperfect welds during printing at the edges, despite the more accurate printer.

These features formed with the Roboze printer can be explained by the target for plastics to be used with the printer.
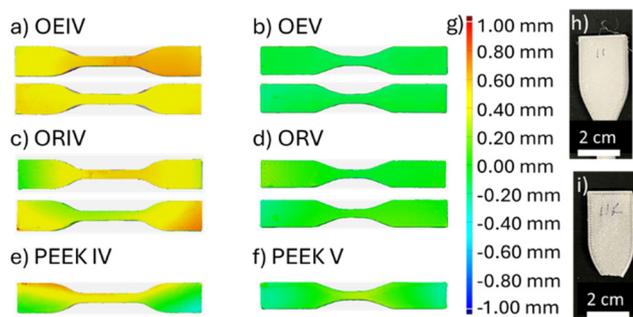
Fig. 5 False color 3D scan of Overture ASTM D638 type IV tensile testing printed on the (a) Ender 3 and (b) Roboze 3D printers, and Overture ASTM D638 type V tensile bars printed on the (c) Ender 3 and (d) Roboze 3D printers. The top of each sample is the upper image, and the part of the sample that touches the build plate is the bottom image in each pair. The Roboze printer was used to print PEEK in (e) type IV and (f) type V ASTM D638 tensile bars. (g) Color bar legend for parts a–f. Photos of grips region of type 4 tensile bars after aging for the equivalent of 1 for (h) Ender 3 and (i) Roboze prints.
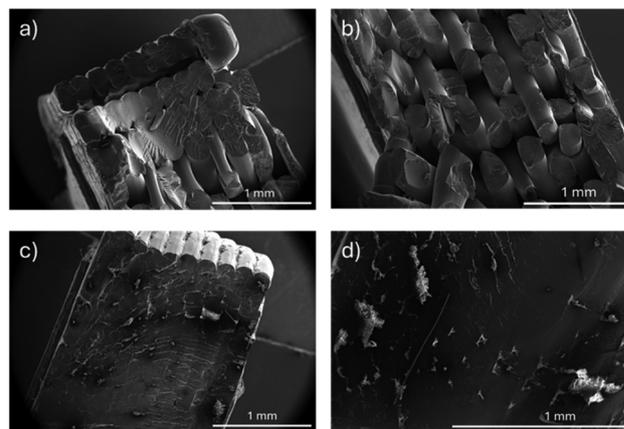
Fig. 6 SEM cross section micrographs of the grips region of O(R)V at (a) perimeter and (b) interior of the tensile bar and analogous micrographs for O(E)V at (c) perimeter and (d) interior of the tensile bar.

The Roboze printer was designed around printing PEEK, which requires high temperatures and crystallization control. To minimize degradation, the length of the hot end is minimized, which is approximately 1.2 cm. The viscosity of PEEK rapidly decreases once the crystals melt to enable facile printing with the type IV tensile bar being more accurate (Fig. 5e) with PEEK than PETG (Fig. 5c). There is a small bend in the type V tensile bar printed with PEEK in the gauge region (Fig. 5f), which is associated with the crystallization stresses slightly warping the sample.

The glass formation region,[63] which is critical to the accuracy in printing of the PETG, extends well beyond T_g and thus the longer time in the melt in the longer hot end (approximately 2.5 cm) of the Ender 3 printer may improve heat transfer to homogenize the temperature of the melt and develop the flow before it exits the hot end. This more homogenous temperature will improve initial flow of the PETG and lead to less obvious roads when examining on the top printed surface as shown in Fig. 5. This also enabled faster optimal print speed (3000 mm s^{-1} for the Ender 3 *versus* 1200 mm s^{-1} for the Roboze printer) and lower optimal bed temperature (75 °C *versus* 80 °C). Attempts to print faster with the Roboze printer failed to generate a cohesive part.

Despite the same extrusion temperature, the morphology of the PETG differs significantly between those printed with the Roboze and Ender printers as shown in Fig. 6. The printed roads appear to be consolidated better at the perimeter (Fig. 6a) than the center of the tensile bar (Fig. 6b) with the Roboze printer. This morphology typically occurs when the printed polymer solidifies quickly.[64] Here, the shorter heated zone in the Roboze printer could limit heat transport leading to extrudate that is cooler than the set temperature.[65] Conversely, the tensile bars printed with the Ender printer show the printed road structure at the perimeter (Fig. 6c) while the center of the tensile bar is mostly consolidated except for

some diamond voids associated with the non-rectangular extrudate from the hot end.

These distinct morphologies lead to significant differences in their mechanical performance. Fig. 7 illustrates representative engineering stress–strain curves from tensile measurements using printed PETG from Overture filaments with the two printers. Without significant aging (1 day), the specimens printed with the Ender yielded and underwent ductile yielding (Fig. 7a), while the specimen printed with the Roboze was brittle and failed at low stress and strain. This significant difference in the performance results from the details of the printer; the print parameters (higher bed temperature and lower print speed) for the Roboze printer favor improved mechanical performance based on prior examination of print parameter optimization, but the shorter hot end appears to lead to weak interfaces between the printed roads (Fig. 6b).

The stress–strain curves for additional printed samples of the Overture filament after physical aging are shown in the ESI in Fig. S7† through S9 for type IV tensile bars and Fig. S10 and S11† for type V tensile bars. The aging of the ductile PETG printed with the Ender results in an increase in the ultimate tensile stress but a reduction in the ductility with the strain to break reducing significantly after effectively one year of aging. At long aging times, an increased strain hardening was observed for the Ender-printed PETG, but aging had limited impact on the stress–strain behavior of the brittle parts printed with the Roboze printer.

Quantification of the mechanical properties as a function of aging time provides insights into how physical aging impacts PETG performance. Fig. 8 illustrates how the elastic modulus, ultimate tensile strength (UTS), and strain at break change under accelerated aging for the Overture filament with both printers. The elastic modulus for the printed PETG is significantly higher with the Ender printer, which is consistent with void defects within the printed structure for the specimens produced with the Roboze printer (Fig. 8a). The voids can be seen *via* SEM imaging in Fig. 6. However, the modulus
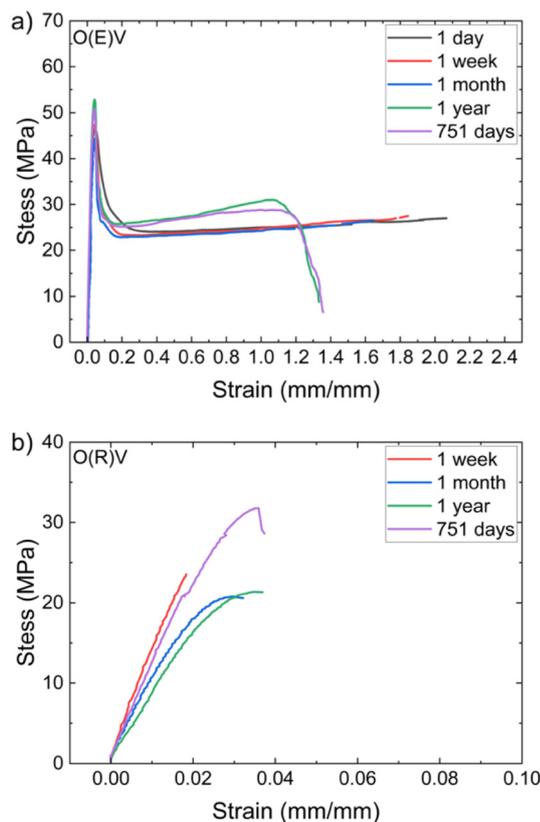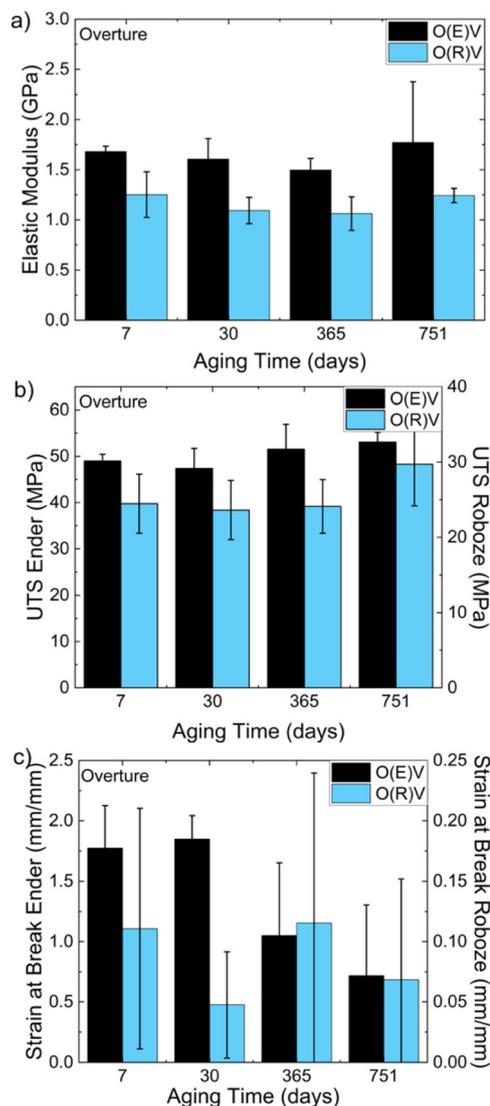
Fig. 7 Representative stress–strain curves as a function of aging time equivalent at 25 °C for the Overture PETG when printed with (a) Ender or (b) Roboze printers.

Fig. 8 Role of printer and aging on the (a) Elastic Modulus, (b) UTS, and (c) elongation at break for printed Overture PETG. The aging is reported as equivalent time at 25 °C based on TTS from the filament.

does not appreciably change on aging. Similarly, the UTS is lower with the Roboze printer (Fig. 8b), but the UTS tends to increase with aging. This is consistent with densification of the PETG during aging. Interestingly, the UTS for the PETG printed with the Ender printer increased consistently with longer aging, similar to the enthalpy recovery measured for the Overture filament (Fig. 4), while the PETG printed with the Roboze exhibited limited aging effects. These results demonstrate that aging of 3D printed parts is dependent on the processing details and optimization of print parameters for a given material is not necessarily globally applicable due to design differences in printers that impact polymer process history.

Aging also tends to reduce the ductility of the printed PETG (Fig. 8c). The large variance in the strain at break results from the stochastic nature of defects that determine failure and the high potential for defect inclusions in MEX printing resulting from the part being comprised effectively of weld lines[66] and interstitial voids from limited plastic flow after printing.[67] However, the influence of the printer selection is greater than aging when considering the mechanical properties. The tensile samples printed on the Roboze printer exhibit lower mechanical properties when compared to those printed on the Ender 3 with the greatest reduction in the elongation at break.

These differences can be ascribed to reduced interlayer adhesion with the Roboze printer, where interlayer adhesion impacts elongation more than other mechanical properties in 3D printed parts.[68,69]

Influence of printing process on aging

In addition to changes in morphology from the details of the print processing, the thermal history of the printed parts is complex due to repeated thermal cycling as plastic is extruded from the hot end next to or on top of previously printed layers. This acts to repeatedly heat local regions for short times.[70] The print path determines the local thermal history as the time between passes of the hotend determines the extent of cooling. The nature of the print path leads to repeated heating and cooling of printed regions that can produce residual stresses and induce local aging in the part as it is printed. These

942 | *RSC Appl. Polym.*, 2025, **3**, 934–947

© 2025 The Author(s). Published by the Royal Society of Chemistry

heating and cooling rates[71] can be significantly greater than the baseline 5 °C min^{-1} used for producing the unaged glass in the DSC experiments (Fig. 2). This thermal history is spatially heterogenous due to the nature of the printing process and could lead to localized differences in aging behavior. Small pieces of the printed PETG were removed from the bottom layer (many hotend passes) and top layer (no interlayer passes) in both the gauge (consistent long time between passes with the hotend) and grip (short time between passes on turning) to probe differences in the aging behavior using the same accelerated aging conditions at 60 °C (Table 3). The locations of the specimens probed by the DSC of the tensile bars are shown schematically in Fig. 9d. The enthalpy recovery after aging was determined by DSC as shown in Fig. S12† for Polymaker, Fig. S13† for Overture, and Fig. S14† for Hatchbox PETG.

Fig. 9 shows the enthalpy loss upon aging of material taken from four locations of a printed ASTM type IV tensile bar for the 3 different filaments. In this case, bottom refers to the layer printed onto the heated bed, and top refers to the last layer of the print. There are several trends that emerge from analysis of the data. First, the enthalpy recovery at intermediate aging times tends to be greater for the bottom of the specimen. This behavior is consistent with the thermal history associated with heating and cooling from the adjacent passing of the hot end during the print process that effectively starts accelerated aging. Second, the gauge region tends to exhibit higher enthalpy recovery than the grip region of the tensile bar at the equivalent of 1 week and 1 month aging at 25 °C. This behavior indicates that the aging of 3D printed plastic parts depends locally on the print path details.

Polymaker PETG, which ages the fastest among the three filament sources, experiences the greatest change in enthalpy at short aging time (Fig. 9a). This behavior is consistent with the temperature history associated with the print path accelerating aging of the PETG. There is a larger change in enthapy with Polymaker as it ages faster and thus the elevated temperature exposures during printing act more aggressively to densify the PETG glass. The enthalpy recovery of the top gauge region appears similar to that for the unstressed state (Fig. 4). However, the enthalpy loss after aging of the printed samples for the equivalent of 1 year appears to be slightly lower than expected. This could be associated with the residual stresses from the print. Printed Overture PETG samples (Fig. 9b) show limited change in the aging at 1 week but there is a general increase in the enthalpy recovery at 1 month in comparison to the unstressed sample (Fig. 4). Hatchbox PETG (Fig. 9c) ages slower but comparison to the unstressed state indicates a significant acceleration in aging (enthalpy loss) as a result of the print process. Interestingly after the equivalent of a year of aging, the enthalpy loss of the 3 printed samples are similar despite the large difference found in the unstressed state (Fig. 4).

Influence of filament source on aging and mechanical properties

Although the printer selection had a more significant impact on properties than physical aging for the Overture PETG as
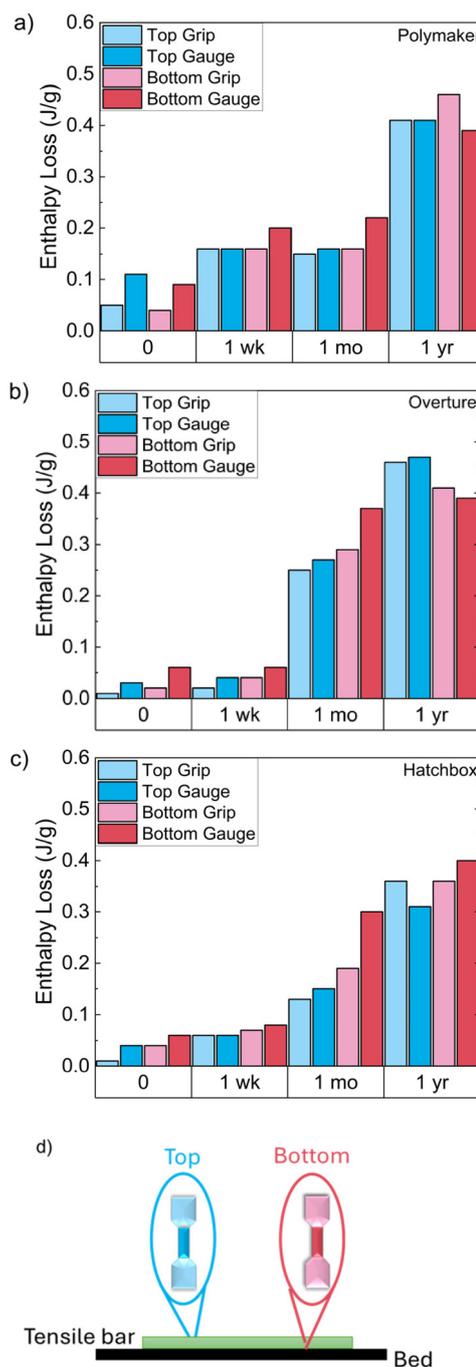

Fig. 9 Enthalpy recovery determined from DSC thermograms on PETG from different locations on printed Type IV tensile bars for (a) Polymaker, (b) Overture and (c) Hatchbox PETG. The location of where the sample was removed from the tensile bar is show in (d), where the colors correspond to the aging data shown in (a–c).

shown in Fig. 8, the tensile strength was found to increase but the PETG embrittles on aging of the printed parts. Fig. 10 illustrates representative stress strain curves for the Hatchbox and Polymaker filaments as a function of aging time and specimen size using the Ender 3 printer. Additional stress–strain curves are included in Fig. S15† through Fig. S18† for these PETG
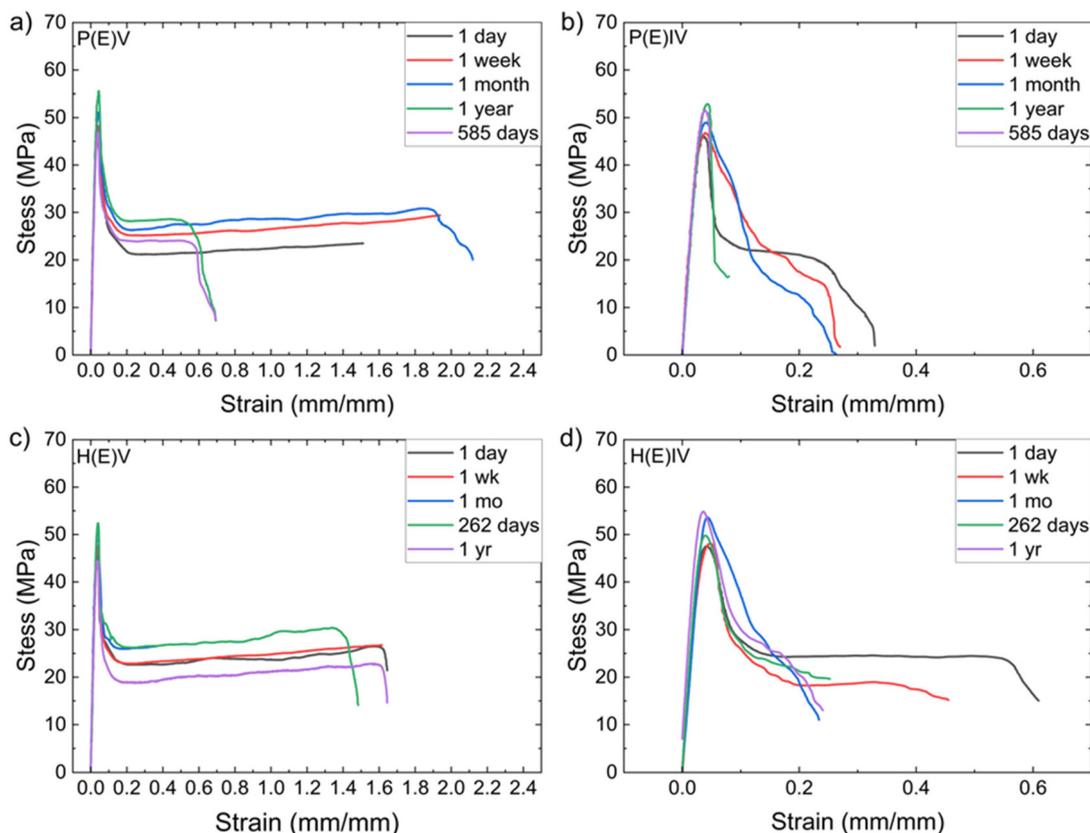
Fig. 10 Representative stress–strain curves for Polymaker (a) type V, P(E)V and (b) type IV P(E)IV as well as Hatchbox (c) type V, H(E)V and (d) type IV, H(E)IV, as a function of effective aging time at 25 °C based on enthalpy recovery.
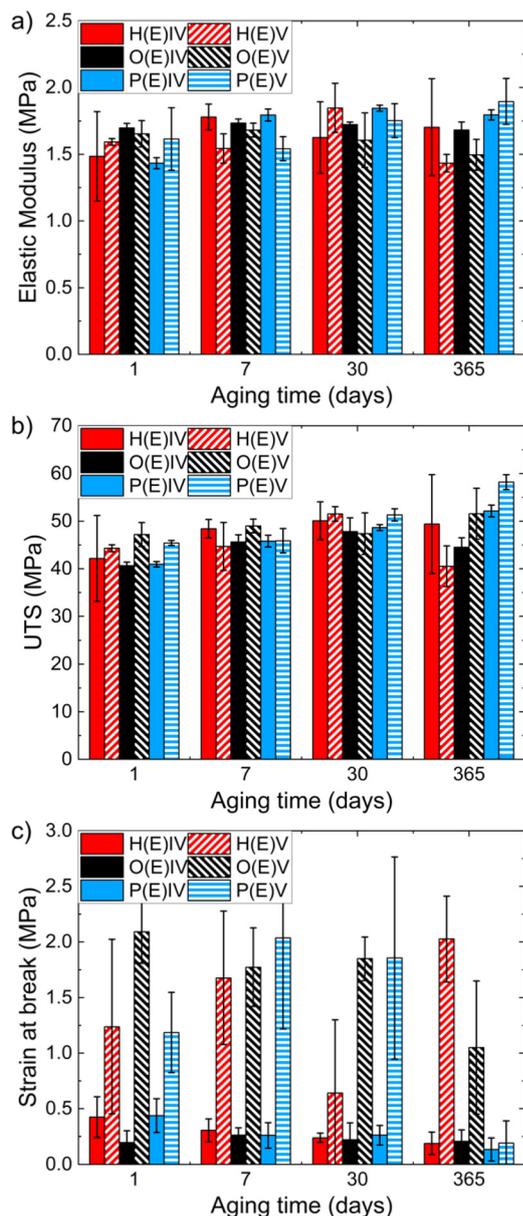
specimens at different aging times. The elastic modulus and UTS are only marginally impacted with the tensile bar size selection (type IV *vs.* type V bars). However, the elongation at break is significantly reduced for the type IV specimens, where failure tends to be nucleated from defects in the printed specimens. Defect probability is increased by the larger size of the gauge,[72] but the increased time between adjacent roads in the print also reduces the interlayer adhesion.[62]

Physical aging of the printed PETG generally leads to an increase in the UTS and a reduction in the strain at break. The extent of these changes is dependent on the filament source. Similar to the Overture PETG, the strain at break for the Polymaker PETG reduces on aging of the type V specimens for the equivalent of 1 year at 25 °C (Fig. 10A). Fig. 10B illustrates that the larger type IV specimens printed using the Polymaker filament exhibit an increase in the tensile strength and reduction in the elongation post yield after aging. In contrast, the type V specimens printed with Hatchbox PETG (Fig. 10c) exhibit almost no reduction in elongation until more than 1 year of aging. This effect does appear to be dependent on the size of the specimen, where the strain at break decreases on aging the Hatchbox PETG with a type IV dog bone. This size effect could be related to the defect probability which increase in a large specimen, but the thermal history is also impacted by the specimen size and this can impact the intralayer weld strength.[62]

When comparing between the filament sources, differences in aging appear to be related to the CHDM content in the PETG; Polymaker has the highest concentrations of CHDM (Table 1) and exhibits the greatest reduction in elongation on aging (Fig. 10a); Overture PETG contains an intermediate CHDM concentration and the ductility of the printed specimens only decreases some on aging (Fig. 6a); Hatchbox PETG contains the least CHDM and exhibits a minor reduction in ductility on aging (Fig. 10c). These differences illustrate that enthalpy recovery does not directly correspond to the physical aging in the mechanical properties as has been reported for other plastics from traditional manufacturing.[17] However for 3D printed specimens, the aging is impacted by details of the processing for the Hatchbox PETG where differences in the aging are observed dependent on the selection of the tensile specimen size (Fig. 10c and d).

Fig. 11 provides a summary of the changes in mechanical properties on aging of the printed PETG for the Ender printer with both type IV and V tensile specimens. The elastic modulus in general does not statistically change with aging (Fig. 11a).[73] The modulus for the Overture PETG is the most consistent across specimen size and aging times. While there is a small trend towards increasing modulus with aging time with the other two PETG, the changes are small. The tensile strength tends to increase with aging with the type V tensile

944 | *RSC Appl. Polym.*, 2025, **3**, 934–947

© 2025 The Author(s). Published by the Royal Society of Chemistry

Fig. 11 Impact of aging on (a) elastic modulus, (b) ultimate tensile strength, and (c) strain at break for the different filament sources.

CHDM also impacts T_g, so the quench depth is greater for the Hatchbox at the same temperature when comparing to the other PETG, which would be consistent with a reduced aging rate. The inclusion of CHDM also acts to increase molecular mobility, which also would accelerate aging. TTS[44] was used for accelerated aging at 60 °C to achieve the equivalent of 1 week, 1 month, and 1 year of aging at 25 °C shown in Table 3, but the printing process leads to a distribution of aging in a single part due to complex thermal history that depends spatially on the print path. These effects may be involved in the changes in the mechanical properties of the PETG not tracking directly with the enthalpy recovery determined from the filament materials. These experiments demonstrate the potential role of physical aging under controlled conditions on the long-term performance of additively manufactured plastic parts. However, humidity could lead to degradation in PETG[74] or facilitate structural re-arrangement to accelerate aging. Initial experiments at 60 °C, 80% relative humidity (Fig. S19 and S20†) demonstrated no statistical change in the mechanical properties of printed PETG after aging in a humid environment in comparison to the same printed PETG aged in vacuum. Designs for durable plastic products produced with additive manufacturing should consider how these products age, which may be dependent on design and print details that impact the thermal history.

Conclusions

Physical aging of additively manufactured PETG results in changes in the mechanical properties. This aging is dependent on the composition of the PETG copolymer, in particular the CHDM concentration. Through examination of the enthalpy recovery in three commercial PETG filaments, the rate of aging increases as the CHDM concentration in the PETG copolymer increases. This dependency was attributed to increased segmental mobility of the more flexible CHDM monomer. The tensile properties of the 3D printed PETG depend on the filament sourcing, size of the test specimen, and the printer used in the manufacture. These differences are associated with the segmental dynamics that control the quality of the intra- and inter-layer adhesion and the associated thermal history for the part. The aging as determined by enthalpy recovery is spatially dependent within the 3D printed part and a distribution of aging behavior was observed for a single part where the bottom aged faster than the top. The aging of the 3D printed PETG tends to increase the tensile strength and reduce the ductility, but the extent of these changes depends both on the filament sourcing, where higher CHDM concentration in the PETG results in larger changes in the mechanical properties, and the details of the printing process, where stresses developed from the thermal history can accelerate the aging. These results demonstrate the potential pitfalls associated with optimization of process parameters for PETG and other glassy plastics as the mechanical performance will depend on the selection of printer, the sourcing of the filament through addi-

specimens, while there is more variability in the UTS with the type IV tensile specimens (Fig. 11b). The effect of aging on the UTS is much weaker for the Hatchbox PETG, which is consistent with this PETG being more resistant to physical aging. Aging tends to reduce the strain at break (Fig. 11c) but there is high variability, likely due to the stochastic nature of defects that lead to failure. These results demonstrate that the influence of aging on the tensile properties of printed PETG is dependent both on the sourcing of the PETG filament and the part size.

It is important to note that the aging does not scale with molecular weight of the PETG (Table 1). The observed differences in the aging rate are correlated with the CHDM content.

© 2025 The Author(s). Published by the Royal Society of Chemistry

RSC Appl. Polym., 2025, 3, 934–947 | 945

tives and composition in case of copolymers, and the expected lifetime of the functional part where physical aging can lead to premature embrittlement if not carefully examined.

Author contributions

Data availability

The raw data associated with this manuscript are all provided as plots within the pdf associated with the ESI.† The raw data are provided in tabulated form online at DOI: 10.5281/zenodo.15374620.

Conflicts of interest

There are no conflicts to declare.

Acknowledgements

References

1 A. El Magri, K. El Mabrouk, S. Vaudreuil, H. Chibane and M. E. Touhami, *J. Appl. Polym. Sci.*, 2020, **137**, 49087.

2 M. A. Matos, A. M. A. C. Rocha and A. I. Pereira, *Int. J. Adv. Manuf. Technol.*, 2020, **107**, 1993–2005.

3 A. L. Woern, D. J. Byard, R. B. Oakley, M. J. Fiedler, S. L. Snabes and J. M. Pearce, *Materials*, 2018, **11**, 1413.

4 J. S. Chohan, N. Mittal, R. Kumar, S. Singh, S. Sharma, J. Singh, K. V. Rao, M. Mia, D. Y. Pimenov and S. P. Dwivedi, *Polymers*, 2020, **12**, 2250.

5 B. H. Lee, J. Abdullah and Z. A. Khan, *J. Mater. Process. Technol.*, 2005, **169**, 54–61.

6 M. Bremer, L. Janoschek, D. Kaschta, N. Schneider and M. Wahl, *SN Appl. Sci.*, 2022, **4**, 156.

7 T. Chen, G. Jiang, G. Li, Z. Wu and J. Zhang, *RSC Adv.*, 2015, **5**, 60570–60580.

8 A. B. Kibler and J. G. Smith, *Linear polyesters of 1, 4-cyclo-hexanedimethanol and amino-carboxylic acids*, US Pat. 2901466, 1959.

9 S. R. Turner, *J. Polym. Sci., Part A: Polym. Chem.*, 2004, **42**, 5847–5852.

10 M. Parenti, PET *vs.* PETG: The Main Differences, https://all3dp.com/2/pet-vs-petg-differences-simply-explained/, (accessed Oct 1, 2024).

11 T. Chen, W. Zhang and J. Zhang, *Polym. Degrad. Stab.*, 2015, **120**, 232–243.

12 S. Guessasma, S. Belhabib and H. Nouri, *Polymers*, 2019, **11**, 1220.

13 S. Jabarin and E. Lofgren, *J. Appl. Polym. Sci.*, 1994, **53**, 411–423.

14 G. Grause, M. Chien and C. Inoue, *Polym. Degrad. Stab.*, 2020, **181**, 109364.

15 K. T. Tan, C. C. White, D. J. Benatti and D. L. Hunston, *Polym. Degrad. Stab.*, 2008, **93**, 648–656.

16 F. Deflorian, S. Rossi, L. Fedrizzi and C. Zanella, *Prog. Org. Coat.*, 2007, **59**, 244–250.

17 J. R. White, *C. R. Chim.*, 2006, **9**, 1396–1408.

18 R. Tian, K. Li, Y. Lin, C. Lu and X. Duan, *Chem. Rev.*, 2023, **123**, 3007–3088.

19 J. Kluczynski, I. Szachogluchowicz, J. Torzewski, L. Sniezek, K. Grzelak, G. Budzik, L. Przeszlowski, M. Malek and J. Luszczek, *Int. J. Fatigue*, 2022, **165**, 107212.

20 J. M. Hutchinson, *Prog. Polym. Sci.*, 1995, **20**, 703–760.

21 I. M. Hodge, *Science*, 1995, **267**, 1945–1947.

22 L. C. E. Struik, PhD thesis, Delft University of Technology, 1977.

23 L. C. Brinson and T. S. Gates, in *Comprehensive Composite Materials*, ed. A. Kelly and C. Zweben, Pergamon, 2000, pp. 333–368.

24 D. Flore, K. Wegener, D. Seel, C. C. Oetting and T. Bublat, *Composites, Part A*, 2016, **90**, 359–370.

25 X. Colin, G. Teyssedre and M. Fois, in *Handbook of Multiphase Polymer Systems*, ed. A. Boudenne, L. Ibos, Y. Candau and S. Thomas, Wiley, HAL, 2011, pp. 797–841.

26 C. G. Amza, A. Zapciu, F. Baciu, M. I. Vasile and D. Popescu, *Polymers*, 2021, **13**, 4467.

27 T. Chen, J. Zhang and H. You, *RSC Adv.*, 2016, **6**, 102778–102790.

28 T. Romeijn, K. Singh, M. Behrens and G. Paul, *J. Polym. Res.*, 2021, **28**, 352.

29 E. Klompen, T. Engels, L. van Breemen, P. Schreurs, L. Govaert and H. Meijer, *Macromolecules*, 2005, **38**, 7009–7017.

30 K. Aljoumaa and M. Abboudi, *Appl. Phys. A*, 2016, **122**, 6.

31 L. A. G. Gray, S. W. Yoon, W. A. Pahner, J. E. Davidheiser and C. B. Roth, *Macromolecules*, 2012, **45**, 1701–1709.

32 M. Razavi, E. Xing and M. D. Ediger, *Macromolecules*, 2022, **55**, 10043–10051.

33 G. B. McKenna, *J. Phys.: Condens. Matter*, 2003, **15**, S737.

34 H. G. H. van Melick, L. E. Govaert, B. Raas, W. J. Nauta and H. E. H. Meijer, *Polymer*, 2003, **44**, 1171–1179.

35 M. Utz, P. G. Debenedetti and F. H. Stillinger, *Phys. Rev. Lett.*, 2000, **84**, 1471–1474.

36 G. B. McKenna, *Comput. Mater. Sci.*, 1995, **4**, 349–360.

37 R. WimbergerFriedl and J. G. deBruin, *Macromolecules*, 1996, **29**, 4992–4997.

38 A. Das, A. E. C. Marnot, J. J. Fallon, S. M. Martin, E. G. Joseph and M. J. Bortner, *ACS Appl. Polym. Mater.*, 2020, **2**, 911–921.

39 A. Costanzo, R. Spotorno, M. V. Candal, M. M. Fernandez, A. J. Mueller, R. S. Graham, D. Cavallo and C. McIlroy, *Addit. Manuf.*, 2020, **36**, 101415.

40 E. L. Gilmer, D. Anderegg, J. M. Gardner, G. Sauti, E. J. Siochi, S. H. McKnight, D. A. Dillard, C. McIlroy and M. J. Bortner, *Addit. Manuf.*, 2021, **48**, 102412.

41 T. S. Chow, *Polymer*, 1993, **34**, 541–545.

42 Y. Rao, J. Greener, C. A. Avila-Orta, B. S. Hsiao and T. N. Blanton, *Polymer*, 2008, **49**, 2507–2514.

43 Q. Shi, R. Xiao, H. Yang and D. Lei, *Polym. -Plast. Technol. Mater.*, 2020, **59**, 835–846.

44 A. T. Weyhe, E. Andersen, R. Mikkelsen and D. Yu, *Polymer*, 2023, **278**, 125987.

45 N. R. Council, *Accelerated Aging of Materials and Structures: The Effects of Long-Term Elevated-Temperature Exposure*, National Academies Press, Washington, DC, 1996.

46 S. Hong, N.-Y. Park, S. Ju, A. Lee, Y. Shin, J. S. Kim, M.-K. Um, J. W. Yi, H. G. Chae and T. Park, *Polym. Test.*, 2023, **124**, 108086.

47 B. W. Rowe, B. D. Freeman and D. R. Paul, *Polymer*, 2010, **51**, 3784–3792.

48 J. Oreilly and I. Hodge, *J. Non-Cryst. Solids*, 1991, **131**, 451–456.

49 J. Guo, R. Xiao, C. Tian and M. Jiang, *J. Non-Cryst. Solids*, 2018, **502**, 15–21.

50 ASTM D638-14, Standard Test Method for Tensile Properties of Plastics, ASTM International, West Conshohocken, PA, 2014.

51 A. Das, E. L. Gilmer, S. Biria and M. J. Bortner, *ACS Appl. Polym. Mater.*, 2021, **3**, 1218–1249.

52 A. Das, J. S. Bryant, C. B. Williams and M. J. Bortner, *Polym. Rev.*, 2023, **63**, 895–960.

53 A. Gudadhe, N. Bachhar, A. Kumar, P. Andrade and G. Kumaraswamy, *ACS Appl. Polym. Mater.*, 2019, **1**, 3157–3164.

54 S. M. Aharoni, *Macromol. Chem. Phys.*, 1978, **179**, 1867–1871.

55 S. F. Yost, C. W. Pester and B. D. Vogt, *J. Polym. Sci.*, 2024, **62**, 2616–2629.

56 L. M. Nicholson, K. S. Whitley and T. S. Gates, *The Combined Influence of Molecular Weight and Temperature on the Aging and Viscoelastic Response of a Glassy Thermoplastic Polyimid*, NASA, Hampton, VA, 2000.

57 L. Martineau, F. Chabert, G. Bernhart and T. Djilali, presented in part at the ECCM17 – 17th European Conference on Composite Materials, Munich, Germany, 2016-06-26, 2016.

58 K. Cui, Z. Ma, N. Tian, F. Su, D. Liu and L. Li, *Chem. Rev.*, 2018, **118**, 1840–1886.

59 K. T. Gillen, R. Bernstein and D. K. Derzon, *Polym. Degrad. Stab.*, 2005, **87**, 57–67.

60 S. Vyazovkin and K. Chen, *Chem. Phys. Lett.*, 2007, **448**, 203–207.

61 M. Williams, R. Landel and J. Ferry, *J. Am. Chem. Soc.*, 1955, **77**, 3701–3707.

62 J.-R. Ai and B. D. Vogt, *Prog. Addit. Manuf.*, 2022, **7**, 1009–1021.

63 D. S. Simmons, M. T. Cicerone, Q. Zhong, M. Tyagi and J. F. Douglas, *Soft Matter*, 2012, **8**, 11455–11461.

64 P. Sikder, B. Challa and S. Gummadi, *Materialia*, 2022, **22**, 101427.

65 F. Peng, B. D. Vogt and M. Cakmak, *Addit. Manuf.*, 2018, **22**, 197–206.

66 C. S. Davis, K. E. Hillgartner, S. H. Han and J. E. Seppala, *Addit. Manuf.*, 2017, **16**, 162–166.

67 J. Ghorbani, P. Koirala, Y. Shen and M. Tehrani, *J. Manuf. Process.*, 2022, **80**, 651–658.

68 S. Bhandari, R. A. Lopez-Anido and D. J. Gardner, *Addit. Manuf.*, 2019, **30**, 100922.

69 M. Lay, N. L. N. Thajudin, Z. A. A. Hamid, A. Rusli, M. K. Abdullah and R. K. Shuib, *Composites, Part B*, 2019, **176**, 107341.

70 H. Vanaei, M. Shirinbayan, M. Deligant, S. Khelladi and A. Tcharkhtchi, *THERMO*, 2021, **1**, 332–360.

71 R. de Macedo, R. Ferreira and K. Jayachandran, *Rapid Prototyp. J.*, 2019, **25**, 1661–1683.

72 D. Yalcin, Effect of Specimen Geometry on Tensile Testing Results, https://www.admet.com/blog/effect-specimen-geometry-tensile-testing-results/, (accessed Oct 8, 2024).

73 C. A. Chatham, A. Das, T. E. Long, M. J. Bortner and C. B. Williams, *Macromol. Mater. Eng.*, 2021, **306**, 2000599.

74 C. Fiorillo, H. Ohnmacht, P. Reyes, P. Van Steenberge, L. Cardon, D. Hooge and M. Edeleva, *Polym. Degrad. Stab.*, 2023, **217**, 110511.

© 2025 The Author(s). Published by the Royal Society of Chemistry

RSC Appl. Polym., 2025, **3**, 934–947 | **947**